ISBN: 978-3-95450-261-5 ISSN: 2673-7000 doi: 10.18429/JACoW-NAPAC2025-MOP099

X-RAY INSPECTION FOR NON-INVASIVE REAL-TIME BEAM DETECTION*

P. K. Roy†, Z. R. Harvey, E. Albin, S. Upadhyayula, S. G. Heppelmann
PLS directorate, Lawrence Livermore National Laboratory, Livermore, CA, USA

Abstract

We introduce a novel non-destructive X-ray diagnostic technique for real-time proton beam profile monitoring. The method utilizes high-energy X-ray photons (120–180 keV) in the Compton-dominated regime to probe the halo or electron environment surrounding the proton beam. Applied X-rays undergo Klein-Nishina Compton scattering with electrons from the beam-induced ionization and ambient gas, then pass through the beam pipe window to reach a position-sensitive detector. The scattered X-ray intensity distribution directly maps the spatial electron density, providing real-time proton beam profile and halo structure information.

INTRODUCTION

Conventional methods for measuring lower-energy charged particle beams—including Faraday cups [1,2], moving wire scanners [3], and scintillators [4,5]—are invasive techniques that become impractical for higher-energy beams exceeding material damage thresholds due to excessive heat deposition and radiation damage. Proton beams present unique detection challenges due to their large electromagnetic interaction cross-sections [6,7], characteristic energy deposition patterns (Bragg peak [8]), and distinct angular scattering distributions upon material interaction. The situation becomes more complex when beam halo [9,10] is present and the beam passes through varying vacuum conditions in a long transport beamline [11].

Alternative beam detection techniques using spill radiation monitoring [12,13] or beam position monitors [14–16] generate unwanted secondary particles [17,18] and present significant challenges for particle species identification. An established non invasive method—a laser wire scanner [19]—has been successfully employed to profile high energy beams by detecting up-scattered Compton photons off electrons as a laser is scanned across the beam. In this study, we investigate a new non-invasive X-ray inspection counterpart [20–22] as a novel approach for proton beam characterization. X-ray photons exhibit exceptional radiation hardness [23–25], offering substantial advantages over conventional optical or electronic detectors that suffer radiation damage [26–28] when exposed to high-intensity proton beams. However, X-ray scattering cross-sections for protons are significantly smaller than for electrons. In this work, X-ray interaction events are simulated to develop a comprehensive proton beam profile monitoring system.

CONCEPTUAL EXPERIMENTAL SETUP

Figure 1 illustrates the conceptual experimental configuration for non-invasive proton beam diagnostics. A bremsstrahlung X-ray source is positioned external to the vacuum beam tube, generating incident photons that interact with the stainless steel wall through photoelectric absorption and Compton scattering mechanisms. At X-ray energies above 100 keV, Compton scattering becomes the dominant interaction process since the photon energies significantly exceed the K-edge binding energies of steel constituents (Fe: 7.1 keV, Cr: 6.0 keV, Ni: 8.3 keV).

The dominant interaction regime is characterized by the dimensionless energy parameter $\alpha = E_\gamma/(m_e c^2)$, where E_γ is the photon energy and $m_e c^2 = 511\,\text{keV}$ represents the electron rest mass energy. Figure 2 illustrates the calculated dominance boundaries between different scattering mechanisms. In the classical regime ($\alpha < 0.1$, corresponding to $E_\gamma < 51\,\text{keV}$), the photoelectric effect dominates due to its strong energy dependence. The photoelectric cross-section scales [29] approximately as $\sigma_{\text{pe}} \propto Z^{4-5}/E_\gamma^{3-3.5}$, making it particularly significant for low-energy photons interacting with high-Z materials.

The transition regime ($0.1 \geq \alpha < 1$) is characterized by Compton scattering dominance, where the interaction probability becomes relatively independent of atomic number and depends primarily on electron density. At higher energies ($\alpha > 2$, corresponding to $E_\gamma > 1.02\,\text{MeV}$), pair production becomes energetically accessible and eventually dominates the interaction cross-section.

For effective penetration of the steel beam pipe, an X-ray source with energies exceeding 100 keV is required to operate within the Compton-dominated regime. The photon flux must be sufficiently high to ensure adequate interaction statistics for reliable measurements. Critical design parameters include detector placement distance, spatial resolution, and detection efficiency, which directly influence system sensitivity and measurement precision. These parameters have been studied through preliminary simulation.

X-RAY SCATTERING PHYSICS

When higher-energy X-rays are applied to conducting metals, the X-rays readily photo-ionize K-shell electrons from all constituent elements, resulting in strong X-ray absorption and the production of characteristic fluorescence X-rays from these elements. However, a significant portion of the primary X-rays (I_0) can still be transmitted through steel, depending on thickness as described by the Beer-Lambert law ($I = I_0 e^{-\mu x}$, where μ is the linear attenuation coefficient

* LLNL-PROC-2009413
† roy28@llnl.gov

ISBN: 978-3-95450-261-5 ISSN: 2673-7000 doi: 10.18429/JACoW-NAPAC2025-MOP099

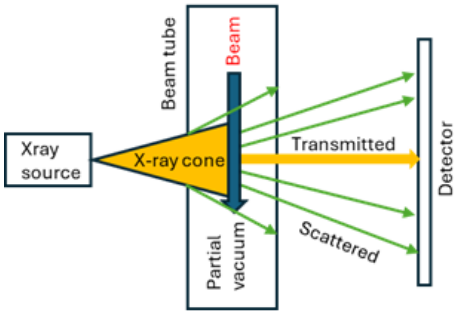

Figure 1: Conceptual experimental setup for non-invasive proton beam diagnostics. High-energy protons propagate through a stainless steel vacuum tube (wall thickness: 1.27 mm). A bremsstrahlung X-ray source is positioned external to the beam pipe, while a position-sensitive detector is located on the opposite side to capture scattered X-ray photons.

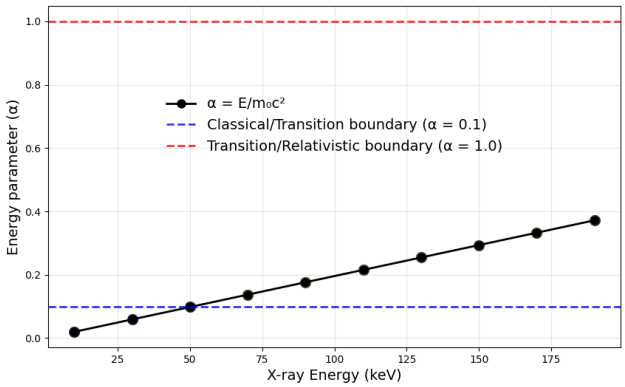

Figure 2: Dimensionless energy parameter $\alpha = E_\gamma/(m_e c^2)$ versus X-ray photon energy E_γ. Dotted lines delineate the classical ($\alpha < 0.1$), transition ($\alpha \geq 0.1$ and $\alpha < 1$), and relativistic ($\alpha > 2$) regimes for photon-matter interactions.

and x is the thickness; the negative exponent indicates that intensity decreases with thickness). In the Compton regime, photons retain significant energy after initial scattering with wall electrons, leading to characteristic angular distributions determined by the Klein-Nishina formula.

The total Compton cross-section, given by the full Klein-Nishina formula [30], is:

$$\sigma_{KN} = 2\pi r_e^2 \left[\frac{1+\alpha}{\alpha^2} \left(\frac{2(1+\alpha)}{1+2\alpha} - \frac{\ln(1+2\alpha)}{\alpha} \right) + \frac{\ln(1+2\alpha)}{2\alpha} - \frac{1+3\alpha}{(1+2\alpha)^2} \right] \quad (1)$$

where r_e is the classical electron radius, $\alpha = h\nu/m_e c^2$ is the dimensionless photon energy parameter, ν is the photon frequency, and h is Planck's constant. It is well known that the Klein-Nishina formalism provides two distinct cross-sections: the total cross-section (units: area, typically cm^2 or barns) used for photon attenuation calculations, radiation dose estimations, and shielding design; and the differential cross-section (units: area per solid angle, cm^2/steradian) employed for analyzing scattered photon energy spectra, angular distributions, and detector response modeling.

The Klein-Nishina differential cross-section for electron scattering [31] can be written in terms of the scattered photon energy parameter:

$$\frac{d\sigma}{d\Omega} = \frac{r_e^2}{2} \left(\frac{E'}{E} \right)^2 \left[\frac{E}{E'} + \frac{E'}{E} - \sin^2\theta \right] \quad (2)$$

where $r_e = e^2/(4\pi\epsilon_0 m_e c^2)$ is the classical radius of the electron, E is the incident photon energy, and E' is the scattered photon energy. In general, the Klein-Nishina formula is most frequently written using wavelength ratios rather than energy ratios ($\lambda/\lambda' = E'/E$). The scattered photon energy (E') is given by the Compton formula:

$$E' = \frac{E}{1 + \frac{E}{m_e c^2}(1-\cos\theta)} = \frac{150\,\text{keV}}{1 + 0.29(1-\cos\theta)} \quad (3)$$

where $E = 150$ keV represents the incident X-ray energy, and θ is scattered angle.

Thomson scattering becomes relevant alongside Compton scattering in the transition regime ($\alpha \approx 0.1$–0.5, 50 keV–250 keV) for broad-spectrum sources, with Klein-Nishina theory providing unified treatment across all energy ranges. The Thomson cross-section [32] for electrons is $\sigma_e = 8\pi r_e^2/3$. Accounting for the mass difference, the proton Thomson cross-section becomes $\sigma_p = \sigma_e \times (m_e/m_p)^2 \approx \sigma_e \times 2.97 \times 10^{-7}$. The differential cross-section is given by:

$$\frac{d\sigma_e}{d\Omega} = r_e^2 \frac{1+\cos^2\theta}{2} \quad (4)$$

where the mass factor 2.97×10^{-7} scales electron differential cross-sections to obtain proton values.

Figure 3 shows X-ray detector [33] images from Compton scattering through 1.27 mm thick stainless steel beam pipe walls without proton beam interaction. The simulation uses Klein-Nishina cross-sections with realistic geometric factors, modeling an X-ray source with photon flux of $\Phi_0 = 10^8$ photons/cm^2/s. Energies span 120–180 keV with optimized weighting for enhanced identification: 30%/40%/30% at 130/150/170 keV energies, respectively.

The X-ray source is positioned 15 cm upstream with cone beam geometry characterized by half-angle $\theta_{\text{cone}} = 0.05$ rad and 1 mm spot size. The cylindrical tube has an inner radius of 5.0 cm, containing hydrogen gas (H_2) at ultra-high vacuum pressure of 10^{-7} Torr. This configuration yields electron densities of $n_e^{\text{wall}} = 8.6 \times 10^{29}$ electrons/m^3 in the stainless steel wall and $n_e^{\text{gas}} = 6.48 \times 10^{15}$ electrons/m^3 in the hydrogen gas. A pixelated detector with active area of 8×8 cm^2, 128×128 pixels, and 90% detection efficiency is positioned 15 cm downstream to record scattered photons.

The detected intensity incorporates geometric factors accounting for beam divergence from the source (r_{source}^{-2}) and solid angle subtended by detector pixels (r_{detector}^{-2}), where r_{source} and r_{detector} represent distances from the scattering volume to the X-ray source and detector, respectively. Wall

ISBN: 978-3-95450-261-5 ISSN: 2673-7000 doi: 10.18429/JACoW-NAPAC2025-MOP099

scattering dominates with greater than 99.9% contribution over gas scattering, producing characteristic ring patterns with peak signals of approximately 10^2 photons/s/pixel, making this technique well-suited for non-invasive beam pipe diagnostics.

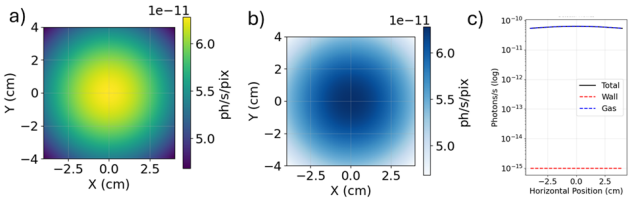

Figure 3: X-ray scattering from cylindrical tube with residual H_2 gas but without protons. (a) Total scattering for combined wall and gas scattering without the proton beam ring pattern; (b) Gas scattering: isolated H_2 gas scattering (uniform, low signal at 10^{-7} Torr); (c) Detector profile: wall scattering dominance over gas background.

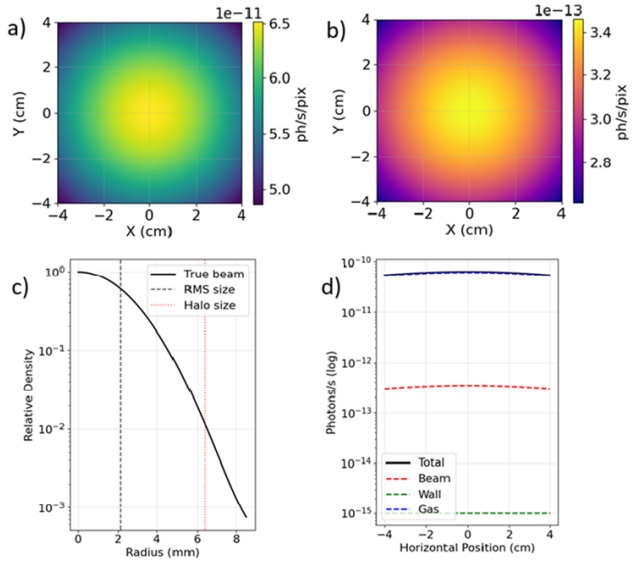

Figure 4: X-ray scattering analysis for proton beams: (a) Total scattering from all electron sources; (b) Isolated beam scattering from space charge, halo, and ionization electrons; (c) reconstructed beam profile showing core and halo structure; (d) detector intensity profiles in the horizontal axis.

Figure 4 shows the X-ray detection results including the proton beam. The diagnostic method monitors an 800 MeV pulsed proton beam delivering 7.5×10^{12} protons per 2 µs pulse (equivalent to 0.6 A peak current) with a 2.13 mm RMS beam radius. The beam creates localized electron populations through residual gas ionization within the beam path, though the precise electron density depends on complex beam-plasma interactions and requires detailed modeling of ionization, recombination, and transport processes.

Three distinct electron sources contribute to the X-ray scattering: steel wall electrons (8.6×10^{29} e$^-$/m^3), hydrogen gas electrons (6.48×10^{15} e$^-$/m^3) distributed throughout the tube interior, and beam-induced electrons localized within the beam envelope. The simulation reveals that wall scattering dominates the signal (> 99.9%) due to the exceptionally high electron density in steel, creating a strong cylindrical background pattern. Beam-induced electrons contribute a small but spatially-correlated signal essential for proton beam profile reconstruction. If the work station is known, X-rays transport window (DD-G-451 glass quality) can be used to reduce steel electrons to have better projection of the gas cloud and beam halo electrons.

Peak detector signals reach 10^2–10^3 photons/s/pixel when exposed, assuming a silicon detector with ∼80% quantum efficiency. Beam profiling is achieved by measuring deviations from the azimuthally symmetric reference pattern without beam. When a proton beam traverses the path, the resulting ionization creates a cylindrical region of enhanced electron density with radius ∼1 mm (determined by secondary electron range). This localized perturbation breaks the azimuthal symmetry, producing angle-dependent intensity variations in the detected X-ray scatter pattern that directly encode the beam's transverse position and profile.

The data presented here, without modest verification, represent preliminary proof-of-concept procedure with simplified analysis to demonstrate the feasibility of this indirect monitoring approach.

CONCLUSION

We present a novel non-destructive diagnostic technique for proton beam profile monitoring based on X-ray Compton scattering tomography. The method employs 150 keV X-rays to probe transient electron density enhancements created by 800 MeV proton beams with halo type environment, enabling indirect beam characterization through analysis of azimuthal asymmetries in the scattered radiation field.

Numerical simulations using Python-based physics models demonstrate feasibility of reconstructing beam profiles. This approach addresses fundamental limitations of conventional beam diagnostics in high-intensity environments: (i) elimination of interceptive elements that suffer radiation damage and activation; (ii) preservation of ultra-high vacuum conditions by avoiding physical beam interaction; and (iii) continuous monitoring capability without beam interruption or halo generation. The technique is particularly suited for next-generation high-power accelerator facilities where material degradation and thermal management constrain traditional diagnostics. Experimental demonstration, systematic characterization and image reconstruction algorithms may validate the work better.

ACKNOWLEDGMENTS

This work was performed under the auspices of the U.S. Department of Energy by Lawrence Livermore National Laboratory under Contract DE-AC52-07NA27344.

ISBN: 978-3-95450-261-5 ISSN: 2673-7000 doi: 10.18429/JACoW-NAPAC2025-MOP099

REFERENCES

[1] P. Strehl, "Beam Loss Monitors," in *Handbook of Accel. Phy. and Eng.*, 2nd ed., A. W. Chao and M. Tigner, Eds., World Scientific, Singapore, 2006, pp. 571–578. doi:10.1142/8543

[2] P. Forck, "Beam Instrumentation and Diagnostics," in *Proc. CERN Accel School: Beam Diagnostics*, CERN-2011-007, Geneva, Switzerland, May 2008, pp. 187–228. doi:10.48550/arXiv.2009.10411

[3] R. M. Jones *et al.*, "X-band RF System for the Int. Linear Collider," in *Proc. EPAC'04*, Lucerne, Switzerland, Jul. 2004, pp. 2625–2627.

[4] R. Ischebeck *et al.*, "Diagnostics for Fourth-Generation Light Sources," *Nucl. Instrum. Methods Phys. Res. A*, vol. 593, no. 3, pp. 455–463, Aug. 2008. doi:10.1016/j.nima.2008.05.052

[5] J. Bergoz, "RF BPMs," in *Proc. CERN Accelerator School: Beam Diagnostics*, CERN-2011-007, Geneva, Switzerland, May 2008, pp. 229–264.

[6] H. Wiedemann, *Particle Accelerator Physics*, 4th ed., Springer, Berlin, 2015. doi:10.1007/978-3-319-18317-6

[7] Particle Data Group, "Review of Particle Physics," *Prog. Theor. Exp. Phys.*, vol. 2022, no. 8, Art. no. 083C01, Aug. 2022. doi:10.1093/ptep/ptac097

[8] H. Paganetti *et al.*, "Accurate Monte Carlo Simulations for Nozzle Design, Commissioning and Quality Assurance for a Proton Radiation Therapy Facility", *Med. Phys.*, vol. 29, no. 10, pp. 2107-2127, 2002. doi:10.1118/1.1762792

[9] T. P. Wangler and K. R. Crandall, "Beam Halo in Proton Linac Beams," in *Proc. LINAC'00*, Monterey, CA, USA, Aug. 2000, pp. 553–557.

[10] A. V. Fedotov, "Beam Loss and Halo Formation in High Intensity Rings," in *Proc. PAC'03*, Portland, OR, USA, May 2003, pp. 1893–1895.

[11] P. K. Roy *et al.*, "Comparison of Profile Measurements and TRANSPORT Beam Envelope Predictions Along the 80-m LANSCE pRad Beamline," *J. Phys.: Conf. Ser.*, vol. 1067, no. 6, Art. no. 062002, Sep. 2018. doi:10.1088/1742-6596/1067/6/062002

[12] A. Fasso *et al.*, "FLUKA: A Multi-Particle Transport Code (Program Version 2005)," *CERN Yellow Reports: Monographs*, CERN-2005-010, INFN/TC_05/11, SLAC-R-773, Geneva, Switzerland, 2005. doi:10.2172/877507

[13] B. J. Holzer, "Collimators and Beam Absorbers," in *Proc. CERN Accelerator School: Beam Diagnostics*, Dourdan, France, May 2006, Rep. CERN-2008-005, pp. 351–395.

[14] R. E. Shafer, "Beam Position Monitoring," in *Proc. AIP Conf.*, vol. 252, 1992, pp. 26–58. doi:10.1063/1.41980

[15] P. Forck *et al.*, "Profile Measurement by Beam Induced Fluorescence for 60 MeV/u to 750 MeV/u Heavy Ion Beams," in *Proc. EPAC'06*, Edinburgh, UK, Jun. 2006, pp. 1013–1015.

[16] P. K. Roy *et al.*, "Proton Beam Position Measurement in Air Using a Beam Position Monitor," *AIP Advances*, vol. 10, no. 9, p. 095023, Sep. 2020. doi:10.1063/5.0021497

[17] R. Assmann *et al.*, "The final collimation system for the LHC," CERN, Geneva, Switzerland, Rep. CERN-LHC-PROJECT-REPORT-919, 2006.

[18] N. V. Mokhov, "Particle production for a muon storage ring I," *Nucl. Instrum. Methods Phys. Res. A*, vol. 472, no. 3, pp. 546–551, 2001. doi:10.1016/S0168-9002(01)01307-9

[19] S. T. Boogert *et al.*, "Micron-scale laser-wire scanner for the KEK Accelerator Test Facility extraction line," *Phys. Rev. Accel. Beams*, vol. 13, p. 122801, Dec. 2010. doi:10.1103/PhysRevSTAB.13.122801

[20] W. C. Röntgen, "On a New Kind of Rays," *Nature*, vol. 53, pp. 274–276, Jan. 1896. doi:10.1038/053274b0

[21] A. H. Compton, "A Quantum Theory of the Scattering of X-Rays by Light Elements," *Phys. Rev.*, vol. 21, no. 5, pp. 483–502, May 1923. doi:10.1103/PhysRev.21.483

[22] A. H. Compton and S. K. Allison, *X-Rays in Theory and Experiment*, 2nd ed., Van Nostrand, New York, NY, USA, 1935. doi:10.1126/science.82.2116.64

[23] T. P. Ma and P. V. Dressendorfer, *Ionizing Radiation Effects in MOS Devices and Circuits*, John Wiley & Sons, New York, NY, USA, 1989. doi:10.1148/radiology.174.3.886

[24] E. Fretwurst *et al.*, "Bulk Damage Effects in Silicon Detectors," *Nucl. Instrum. Methods Phys. Res. A*, vol. 326, no. 1–2, pp. 357–365, Mar. 1993. doi:10.1016/S0168-9002(96)00668-7

[25] K. A. LaBel *et al.*, "Proton-Induced Transients," *IEEE Trans. Nucl. Sci.*, vol. 44, no. 6, pp. 1885–1892, Dec. 1997. doi:10.1109/23.658957

[26] M. T. Robinson, "Basic Physics of Radiation Damage Production," *J. Nucl. Mater.*, vol. 216, pp. 1–28, Oct. 1994. doi:10.1016/0022-3115(94)90003-5

[27] G. H. Kinchin and R. S. Pease, "The Displacement of Atoms in Solids by Radiation," *Rep. Prog. Phys.*, vol. 18, no. 1, pp. 1–51, Jan. 1955. doi:10.1088/0034-4885/18/1/301

[28] G. P. Summers *et al.*, "Damage correlations in semiconductors exposed to gamma, electron and proton radiations," *IEEE Trans. Nucl. Sci.*, vol. 40, no. 6, pp. 1372–1379, Dec. 1993. doi:10.1109/23.273529

[29] R. H. Pratt, A. Ron, and H. K. Tseng, "Atomic Photoelectric Effect Above 10 keV," *Rev. Mod. Phys.*, vol. 45, no. 2, pp. 273–325, Apr. 1973. doi:10.1103/RevModPhys.45.273

[30] A. T. Nelms, "Graphs of the Compton Energy-Angle Relationship and the Klein-Nishina Formula from 10 keV to 500 MeV," NIST Circular 542, National Bureau of Standards, U.S. Department of Commerce, Washington, DC, USA, 1953.

[31] R. D. Evans, *The Atomic Nucleus*, McGraw-Hill, New York, NY, USA, 1955, pp. 674–676.

[32] J. D. Jackson, *Classical Electrodynamics*, 3rd ed., John Wiley & Sons, New York, NY, USA, 1998, ch. 14, p. 695. doi:10.1002/3527600434.eap109

[33] S. Del Sordo *et al.*, "Progress in the Development of CdTe and CdZnTe Semiconductor Radiation Detectors," *Sensors*, vol. 9, no. 5, pp. 3491–3526, May 2009. doi:10.3390/s90503491